Dalton Transactions

ROYAL SOCIETY OF CHEMISTRY

PAPER

View Article Online
View Journal | View Issue

Cite this: *Dalton Trans.*, 2025, **54**, 12018

Spectroscopic, structural and photophysical characterization of chloro-bridged iridium(III) and rhodium(III) dinuclear complexes with 1-phenyl-1*H*-pyrazole and their analogues with 1-(2,4-difluorophenyl)-1*H*-pyrazole†

Patryk Wójcik, [a] Camille Latouche, *[b,c] Kinga Suwińska [d] and Anna Kamecka *[a]

Received 16th May 2025,
Accepted 7th July 2025

DOI: 10.1039/d5dt01156f

rsc.li/dalton

This paper deals with the synthesis and spectroscopic characterization of four important precursors, dinuclear $[(C^N)_2Ir\text{-}\mu\text{-}Cl]_2$ and $[(C^N)_2Rh\text{-}\mu\text{-}Cl]_2$ complexes, containing deprotonated 1-phenyl-1*H*-pyrazole or 1-(2,4-difluorophenyl)-1*H*-pyrazole as cyclometallating (C^N) ligands. The molecular structures of these μ-chloro-bridged complexes were confirmed by X-ray crystallography. These complexes showed luminescence in 1 : 1 MeOH/EtOH glasses at 77 K but were non-emissive in dichloromethane solutions at room temperature. A time-dependent DFT (TDDFT) study was conducted to gain insights into the electronic structures of these systems.

Introduction

The photophysical properties of iridium(III) coordination compounds make this class of materials very important among transition metal complexes used in optoelectronic and photonic applications[1] such as organic light-emitting diodes (OLEDs)[2–4] and light-emitting electrochemical cells (LEECs).[5–7] Luminescent cyclometallated iridium(III) complexes have also been applied in different biological studies as biomolecular probes, cellular imaging agents, and photodynamic therapeutics.[8–11] Ir(III) photoredox catalysts have also found applications in small-molecule synthesis and integration of other catalytic technologies,[12] as well as in cancer therapy[13,14] and as catalysts for water oxidation.[15–17] Cyclometallated iridium(III) complexes typically exhibit bright emission at room temperature, which can be tuned across the visible spectrum by ligand substitution and combination, display efficient spin–orbit coupling (SOC), leading to high emission quantum yields, possess radiative lifetimes in the microsecond range, and are thermally and chemically stable. The emission seems to originate from metal–ligand-to-ligand charge transfer (^{3}MLLCT) and triplet ligand-centered (^{3}LC) excited states, or a combination of ^{3}MLLCT/^{3}LC states.[18,19]

In turn, Rh(III) complexes are mainly biologically important compounds, as they can act as inhibitors of proteins or modulators of protein–protein interactions and can interact with specific biomolecular targets.[20,21] Complexes of this type show interesting anticancer activity and inhibit certain enzymes and non-enzymatic proteins, such as inflammatory mediators, isomerases, demethylases, kinases, pyrophosphatases/phosphodiesterases, reductases, oxidases, proteases and β-haematin.[22–24] In contrast to Ir(III) complexes, cyclometallated Rh(III) complexes are rather poor emitters with very low emission quantum yields or are non-emissive at room temperature.[24–31] These complexes show emission in solution glass at 77 K, their emission spectra exhibit vibrational structures, and their emission lifetimes at this temperature are long, even up to several milliseconds.[25,26,32–34] In such a temperature regime, the emission originates from an excited state of predominant ^{3}IL, and the lowest excited state from which it occurs can be located on a cyclometallating or an ancillary ligand.

Recently, we have focused on cyclometallated complexes of the type $[M(C^N)_2(N^N)]^+$, in which the central ion was Ir(III)

[a]*University of Siedlce, Faculty of Natural Sciences, 3 Maja 54, 08-110 Siedlce, Poland. E-mail: anna.kamecka@uws.edu.pl*
[b]*Nantes Université, CNRS, Institut des Matériaux de Nantes Jean Rouxel, IMN, F-44000 Nantes, France. E-mail: Camille.Latouche@cnrs-imn.fr*
[c]*Institut Universitaire de France, Paris 75005, France*
[d]*Cardinal Stefan Wyszyński University in Warsaw, Faculty of Mathematics and Natural Sciences, K. Wóycickiego 1/3, 01 938 Warszawa, Poland*

†Electronic supplementary information (ESI) available: ^{1}H and ^{13}C NMR spectra of the Rh(III) dichloro-bridged dinuclear complexes, crystallographic data and refinement parameters, theoretical results and crystallographic data in CIF files for the $[(ppz)_2Ir\text{-}\mu\text{-}Cl]_2$ and $[(dfppz)_2Rh\text{-}\mu\text{-}Cl]_2$ complexes. CCDC 2431406 and 2431407. For ESI and crystallographic data in CIF or other electronic format see DOI: https://doi.org/10.1039/d5dt01156f

($5d^6$) or its isoelectronic Rh(III) ($4d^6$) ion, both located in the same group of the periodic table.[35–37] As C^N ligands, we used 1-phenyl-1*H*-pyrazole or its analogue containing fluorine substituents, 1-(2,4-difluorophenyl)-1*H*-pyrazole, while as ancillary N^N ligands, we used α-diimines. The photophysical properties of these complexes have been studied in detail, and the nature of the excited states from which emission occurs has been explored. Ir(III) and Rh(III) complexes, despite their very similar geometries and other structural features, show very significant differences in their emission properties at both room temperature and 77 K. In contrast to the strongly emissive Ir(III) complexes, the Rh(III) analogues are almost non-emissive at room temperature.

The majority of syntheses of these types of mononuclear Ir(III) and Rh(III) complexes proceed by the formation of a dichloro-bridged intermediate with the general formula $[(C^N)_2Ir\text{-}\mu\text{-}Cl]_2$ or $[(C^N)_2Rh\text{-}\mu\text{-}Cl]_2$, where C^N is a cyclometallating ligand. These dichloro-bridged dinuclear complexes are prepared according to the protocol first reported by Nonoyama.[38] Since then, there have been many reports on the synthesis of these C^N-cyclometallated dinuclear complexes, and more recently, the positive effect of microwave irradiation on the formation of dichloro-bridged iridium(III) dinuclear complexes and the importance of the presence of water in this process have also been proven.[39] A search of the Cambridge Structural Database (CSD, version 2024.3.0)[40] for the dichloro-bridged dinuclear complexes of Ir(III) or Rh(III) metal ions coordinated by cyclometallating ligands revealed more than sixty and ten structures, respectively. More than one-third of these are structures of dichloro-bridged dinuclear complexes containing 2-phenylpyridine or its derivatives, and only four are structures of dinuclear complexes in which the cyclometallating ligand is 1-phenyl-1*H*-pyrazole or its derivative (CSD refcodes: IMIFAM,[41] IQOZJIC,[42] TEPSEO[43] and VIXHEP).[44] However, there are not many papers devoted to their photophysical properties, which are often overlooked, since dichloro-bridged dinuclear complexes are only intermediates in the synthetic route, and the merits of research are the final mononuclear complexes of these metal ions. However, recently, interest in the photophysical properties of dinuclear complexes has increased, as examples of dichloro-bridged iridium(III) complexes used as emissive dopants in OLEDs have been reported in the literature.[45,46]

According to literature data, most dichloro-bridged Ir(III) dinuclear complexes are rather poor emitters at room temperature and show very low emission quantum yields not exceeding a few percent,[25,47–51] with only a few exceptions,[45,46] and their Rh(III) analogues do not emit at this temperature at all.[25,47,52] However, at a temperature of 77 K, both $[(C^N)_2Ir\text{-}\mu\text{-}Cl]_2$ and $[(C^N)_2Rh\text{-}\mu\text{-}Cl]_2$ dinuclear complexes show emission.[25,47,49,51,52] The nature of the emissive states in cyclometallated dichloro-bridged Ir(III) dinuclear complexes is qualitatively different from that in structurally similar Rh(III) complexes. On the basis of previous literature reports, the $[(C^N)_2Rh\text{-}\mu\text{-}Cl]_2$ dinuclear complexes (C^N – 2-phenylpyridine and benzo[*h*]quinoline,[47] 4-(2-pyridyl)benzaldehyde[25] and 2-(2′-thienyl)-pyridine[52]) in glass solution at 77 K display a structured emission band with peak maxima in the range of 510–530 nm, and emission lifetimes at this temperature are long, reaching up to several milliseconds. The 77 K glass emission of these complexes was assigned mainly to an excited state of ^{3}IL ($\pi \rightarrow \pi^*$)(C^N$^-$) character or to this state with some admixture of ^{3}MLCT (d_π(Rh) $\rightarrow \pi^*$(C^N$^-$)) character. In turn, the photoluminescence of $[(C^N)_2Ir\text{-}\mu\text{-}Cl]_2$ complexes is characterized by emission from either a predominantly ^{3}MLCT state, a predominantly ^{3}LC state or a mixed ^{3}LC/^{3}MLCT state.

During our previous studies focused on the structural and photophysical properties of mononuclear $[Ir(C^N)_2(N^N)]^+$ and $[Rh(C^N)_2(N^N)]^+$ type complexes, we observed that the emission spectra of dichloro-bridged dinuclear complexes of the Rh(III) metal ion at 77 K are slightly different from those reported in the literature and, to our surprise, show a bathochromic shift relative to the spectra of their Ir(III) analogues. Such an effect suggests a different nature of the excited state from which emission occurs. We therefore decided to investigate the photoluminescence properties of all dichloro-bridged dinuclear complexes in more detail.

Herein, we report the synthesis, structural, spectroscopic and photophysical characterization of four dinuclear complexes with a general structure of $[(C^N)_2Ir\text{-}\mu\text{-}Cl]_2$ or $[(C^N)_2Rh\text{-}\mu\text{-}Cl]_2$ by altering the ligand, C-deprotonated 1-phenyl-1*H*-pyrazole or 1-(2,4-difluorophenyl)-1*H*-pyrazole (L = ppz$^-$ or dfppz$^-$) (Scheme 1). To determine the emitting state, experimental studies were carried out together with (TD-)DFT computations.

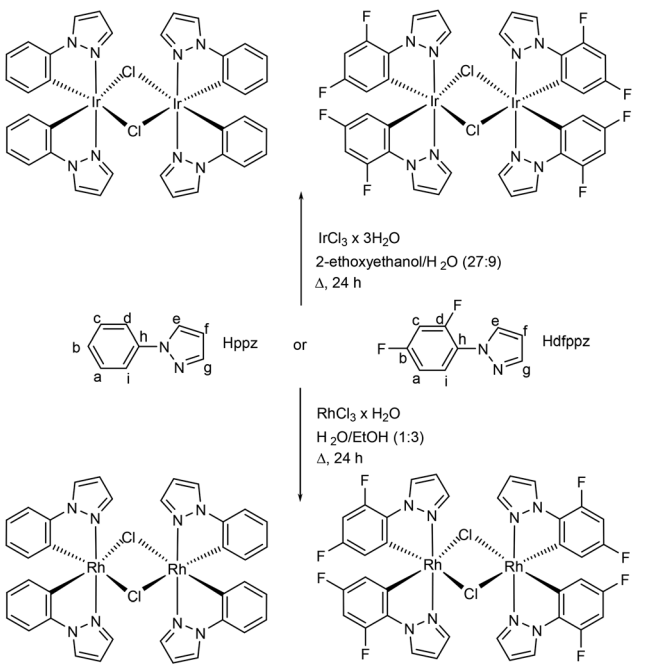

Scheme 1 Synthesis conditions and chemical structures of the investigated $[(ppz)_2Ir\text{-}\mu\text{-}Cl]_2$, $[(dfppz)_2Ir\text{-}\mu\text{-}Cl]_2$, $[(ppz)_2Rh\text{-}\mu\text{-}Cl]_2$ and $[(dfppz)_2Rh\text{-}\mu\text{-}Cl]_2$ complexes (Hppz – 1-phenyl-1*H*-pyrazole, Hdfppz – 1-(2,4-difluorophenyl)-1*H*-pyrazole).

Results and discussion

Synthesis and structures of dichloro-bridged $[(C^N)_2Ir\text{-}\mu\text{-}Cl]_2$ and $[(C^N)_2Rh\text{-}\mu\text{-}Cl]_2$ dinuclear complexes

The synthetic routes and structures of the employed dichloro-bridged $[(ppz)_2Ir\text{-}\mu\text{-}Cl]_2$, $[(dfppz)_2Ir\text{-}\mu\text{-}Cl]_2$, $[(ppz)_2Rh\text{-}\mu\text{-}Cl]_2$ and $[(dfppz)_2Rh\text{-}\mu\text{-}Cl]_2$ dinuclear complexes are depicted in Scheme 1. Their ^1H and ^{13}C NMR spectra were recorded in non-polar and non-coordinating CD_2Cl_2 solution to avoid their cleavage by coordinating solvent and conversion of the dinuclear complexes to the solvated monomer, which is an equilibrium reaction.[39]

From the overall pattern of the ^1H NMR spectra, it is evident that each of the dichloro-bridged dinuclear complexes possesses similar C_2 symmetry, and therefore, the four cyclometallating ligands are equivalent. As a result, the presence of one set of proton signals from the ppz^- (seven signals) or $dfppz^-$ (five) ligands can be clearly observed in the spectra of the $[(ppz)_2M\text{-}\mu\text{-}Cl]_2$ and $[(dfppz)_2M\text{-}\mu\text{-}Cl]_2$ complexes, respectively (Fig. 1, *cf.* ESI, Fig. S1–S4†). In addition to the absence of the signals of the phenyl protons H_b and H_d (fluorine substituents) in the spectra of $[(dfppz)_2Ir\text{-}\mu\text{-}Cl]_2$ and $[(dfppz)_2Rh\text{-}\mu\text{-}Cl]_2$ complexes, the main difference is the value of the chemical shift of proton H_a. The signal corresponding to this proton, which is attached to the carbon atom of the $dfppz^-$ ligand adjacent to the cyclometallating one and to the carbon substituted with a highly electronegative fluorine atom, is shifted downfield in relation to the corresponding signal of the $[(ppz)_2Ir\text{-}\mu\text{-}Cl]_2$ and $[(ppz)_2Rh\text{-}\mu\text{-}Cl]_2$ spectra, respectively ($\Delta\delta \cong 0.55$ ppm).

In the $^{13}C\{^1H\}$ NMR spectra of all dichloro-bridged dinuclear complexes (Fig. 1, *cf.* ESI, Fig. S1–S4†), the number of signals is adequate to the number of equivalent carbon atoms contained in the molecules of coordinated ppz^- or $dfppz^-$ ligands. A distinctive feature of the spectra of $[(dfppz)_2Ir\text{-}\mu\text{-}Cl]_2$ and $[(dfppz)_2Rh\text{-}\mu\text{-}Cl]_2$, complexes with the fluorine-substituted ligands, is the presence of coupling of the fluorine to the aromatic carbons. The signals of carbon occurring at the chemical shift of about ~149 and ~159 ppm with the highest value of the $J_{C\text{—}F}$ coupling constant of ~250 Hz confirm the presence of fluorine substituents. In turn, a characteristic doublet in $[(ppz)_2Rh\text{-}\mu\text{-}Cl]_2$ and $[(dfppz)_2Rh\text{-}\mu\text{-}Cl]_2$ spectra in the chemical shift range of 148–151 ppm with a $J_{C\text{–}Rh}$ coupling constant of ~36 Hz confirms the cyclometallation of the rhodium(III) ion.

For $[(ppz)_2Ir\text{-}\mu\text{-}Cl]_2$ and $[(dfppz)_2Rh\text{-}\mu\text{-}Cl]_2$ dinuclear complexes, the single-crystal X-ray structures were solved. The perspective views of these dinuclear compounds are shown in Fig. 2, and selected bond distances are tabulated in Table 1. The crystal structure determination revealed that crystals of $[(ppz)_2Ir\text{-}\mu\text{-}Cl]_2$ crystallize in the monoclinic space group $P2_1/n$ and crystals of $[(dfppz)_2Rh\text{-}\mu\text{-}Cl]_2$ crystallize in the monoclinic space group $C2/c$. Molecules of these dinuclear complexes consist of two octahedral iridium(III) or rhodium(III) ions, each ligated by two cyclometallated ppz^- or $dfppz^-$ and two bridging chlorido ligands. The N-donor atoms in these molecules occupy the apical positions in the distorted octahedral coordination sphere, whereas the metal–C bonds of the cyclometalated rings exhibit a mutual *cis* orientation around both central metal ions. The chlorido ligands occupy the equatorial plane in the *trans* position to the cyclometallated C atoms, whereas the nitrogen atoms were confirmed to be mutually *trans* to each other in this arrangement of ligands. The M–C

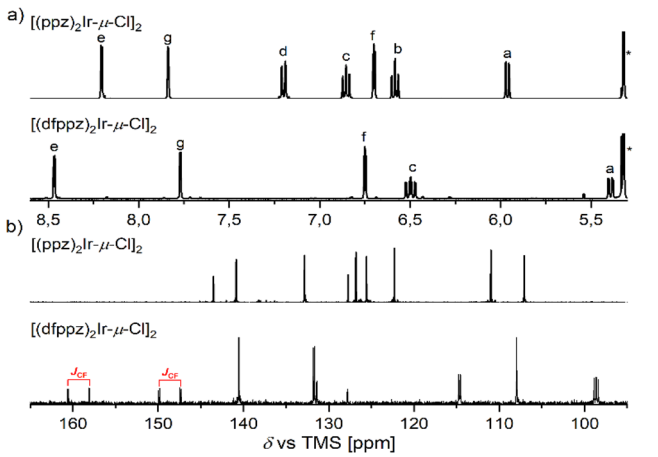

Fig. 1 ^1H NMR (a) and ^{13}C NMR (b) spectra of the dichloro-bridged $[(ppz)_2Ir\text{-}\mu\text{-}Cl]_2$ and $[(dfppz)_2Ir\text{-}\mu\text{-}Cl]_2$ dinuclear complexes. The asterisk * indicates the signals assigned to residual CH_2Cl_2.

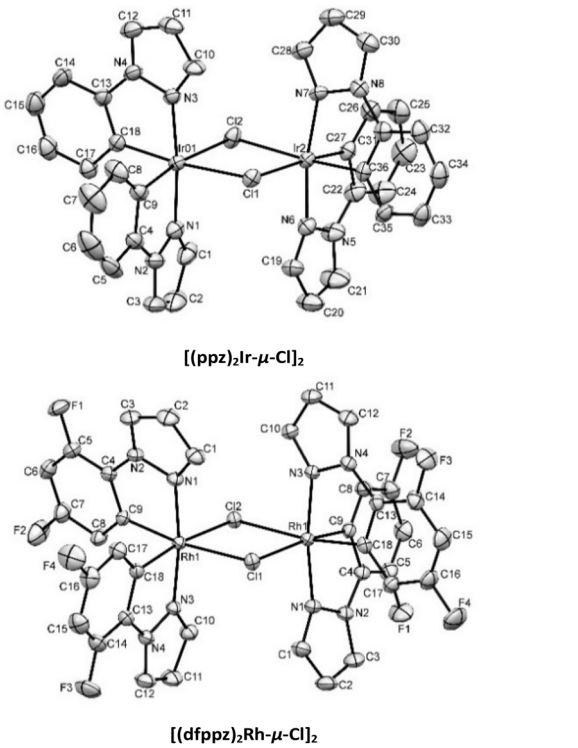

Fig. 2 Molecular structures of $[(ppz)_2Ir\text{-}\mu\text{-}Cl]_2$ (top) and $[(dfppz)_2Rh\text{-}\mu\text{-}Cl]_2$ (bottom) with atomic labelling and displacement ellipsoids drawn at the 30% probability level. Hydrogen atoms are omitted for clarity.

Table 1 Metal–ligand bond lengths (Å) in the S_0 and T_0 states for the investigated $[(ppz)_2M\text{-}\mu\text{-}Cl]_2$ and $[(dfppz)_2M\text{-}\mu\text{-}Cl]_2$ complexes. Data from DFT computations and X-ray investigations

	Metal–ligand bond lengths					
Metal–ligand bond type	X-ray data	CH_2Cl_2 solution S_0	CH_2Cl_2 solution T_0	X-ray data	CH_2Cl_2 solution S_0	CH_2Cl_2 solution T_0
	$[(ppz)_2Ir\text{-}\mu\text{-}Cl]_2$			**$[(dfppz)_2Ir\text{-}\mu\text{-}Cl]_2$**		
Ir1–$C_{C\text{^}N}$	1.988(5)	1.991	1.984	1.999(5)[a]	1.988	1.979
	2.019(5)	1.991	2.001	1.982(6)	1.988	1.999
Ir1–$N_{C\text{^}N}$	2.025(5)	2.023	2.018	2.028(5)	2.023	2.018
	2.027(4)	2.023	2.021	2.032(5)	2.023	2.019
Ir1–Cl	2.4934(12)	2.599	2.526	2.4962(17)	2.584	2.626
	2.5188(13)	2.6	2.624	2.4870(15)	2.585	2.509
Ir2–$C_{C\text{^}N}$	1.999(5)	1.99	2.032	1.989(5)	1.988	2.031
	2.001(5)	1.99	2.033	2.000(6)	1.988	2.033
Ir2–$N_{C\text{^}N}$	2.029(4)	2.025	2.026	2.022(5)	2.022	2.025
	2.032(5)	2.025	2.029	2.014(5)	2.022	2.028
Ir2–Cl	2.4967(12)	2.603	2.579	2.4951(15)	2.586	2.582
	2.5101(13)	2.604	4.298	2.4856(17)	2.587	4.48
	$[(ppz)_2Rh\text{-}\mu\text{-}Cl]_2$			**$[(dfppz)_2Rh\text{-}\mu\text{-}Cl]_2$**		
Rh1–$C_{C\text{^}N}$	1.981(9)[b]	1.984	1.974	1.988(3)	1.983	1.972
	1.975(9)	1.984	1.998	1.997(3)	1.983	1.995
Rh1–$N_{C\text{^}N}$	1.995(7)	2.037	2.028	2.016(2)	2.035	2.027
	2.018(7)	2.037	2.039	2.021(3)	2.035	2.027
Rh1–Cl	2.548(2)	2.619	2.524	2.4863(7)	2.6	2.509
	2.505(3)	2.62	2.667	2.5141(7)	2.601	2.655
Rh2–$C_{C\text{^}N}$	1.991(8)	1.985	2.042		1.983	2.044
	1.97(1)	1.985	2.051		1.983	2.053
Rh2–$N_{C\text{^}N}$	2.022(7)	2.034	2.042		2.032	2.0439
	2.031(7)	2.035	2.044		2.032	2.044
Rh2–Cl	2.522(3)	2.619	2.606		2.6	2.533
	2.514(2)	2.619	4.469		2.601	4.531

[a] X-ray data taken from ref. 43. [b] X-ray data taken from ref. 44.

bond distances (on average, 1.98–2.00 Å) are slightly shorter than the M–N bond distances (on average, 2.02–2.03 Å) in the cyclometallating ligands, and the values are similar to those found in the literature for (C^N)-cyclometallated complexes. Considering the Ir···Ir distance of 3.740(1) Å and the Rh···Rh distance of 3.694(1) Å with respect to the sum of the two ionic radii of 1.64 Å and 1.61 Å, for Ir(III) and Rh(III),[53] respectively, it can be concluded that there is no direct metal–metal bond in these dinuclear complexes. This result and trend is confirmed by DFT calculations, in which Ir···Ir and Rh···Rh are computed at 4.005 and 3.981 Å, respectively. The determined molecular structures of these complexes match the most reported ones of Rh(III) and Ir(III) compounds of this type.[43,44,54–56] Overall, the computed and experimental data are in good agreement, giving us confidence in our computational protocol used to investigate the optoelectronic properties.

In both crystal structures of the studied $[(dfppz)_2Rh\text{-}\mu\text{-}Cl]_2$ and $[(ppz)_2Ir\text{-}\mu\text{-}Cl]_2$ complexes, a number of weak intermolecular interactions were found: C–H···Cl and C–H···F non-classical hydrogen bonds and π···π stacking interactions in the case of the $[(dfppz)_2Rh\text{-}\mu\text{-}Cl]_2$ complex, and C–H···Cl non-classical hydrogen bonds and C–H···π interactions in the case of the $[(ppz)_2Ir\text{-}\mu\text{-}Cl]_2$ complex (Fig. 3 and Tables S1, S2 *cf.* ESI†). The offset π-stacking between cyclometallated ligands is of particular interest because this type of interaction is believed to be responsible for the aggregation-induced phosphorescence emission of iridium(III) and rhodium(III) complexes.[54,57]

Electronic absorption spectra

The UV-Vis absorption data of the studied cyclometallated dichloro-bridged dinuclear complexes in CH_2Cl_2 solutions are presented in Table 2, and the absorption spectra of these complexes are shown in Fig. 4. The simulated spectra using TDDFT on top of the relaxed ground-state geometries are given in Fig. S9 (*cf.* ESI†). The absorption spectral profiles of all complexes are quite similar. They contain strong high-energy absorption bands and shoulders at wavelengths between 225 and 300 nm and low-energy absorption bands within the range of 300–400 nm of rather low intensities. The same results are obtained for the simulated spectra. The high energy bands are attributed to characteristic singlet ligand-centered (^{1}LC) spin-allowed $^1\pi$–π^* transitions. The high-energy maxima of $[(dfppz)_2M\text{-}\mu\text{-}Cl]_2$ dinuclear complexes are shifted hypsochromically by a few nanometers in comparison with the maxima of the bands in the spectra of dinuclear complexes without fluorine substituents in the cyclometallating ligands. At lower energies, the absorption spectra of the Ir(III) as well as Rh(III) dinuclear complexes are dominated by spin-allowed metal-to-ligand charge transfer (^{1}MLCT) transitions and intra-ligand charge transfer (^{1}ILCT) transitions, as reported for similar cyclometallated complexes.[25,46,47,51,54] By analyzing the positions of the band maxima, two distinct effects can be seen. The absorption bands of the rhodium(III) dichloro-bridged dinuclear complexes (λ_{abs} = 313–331 nm) are blue-

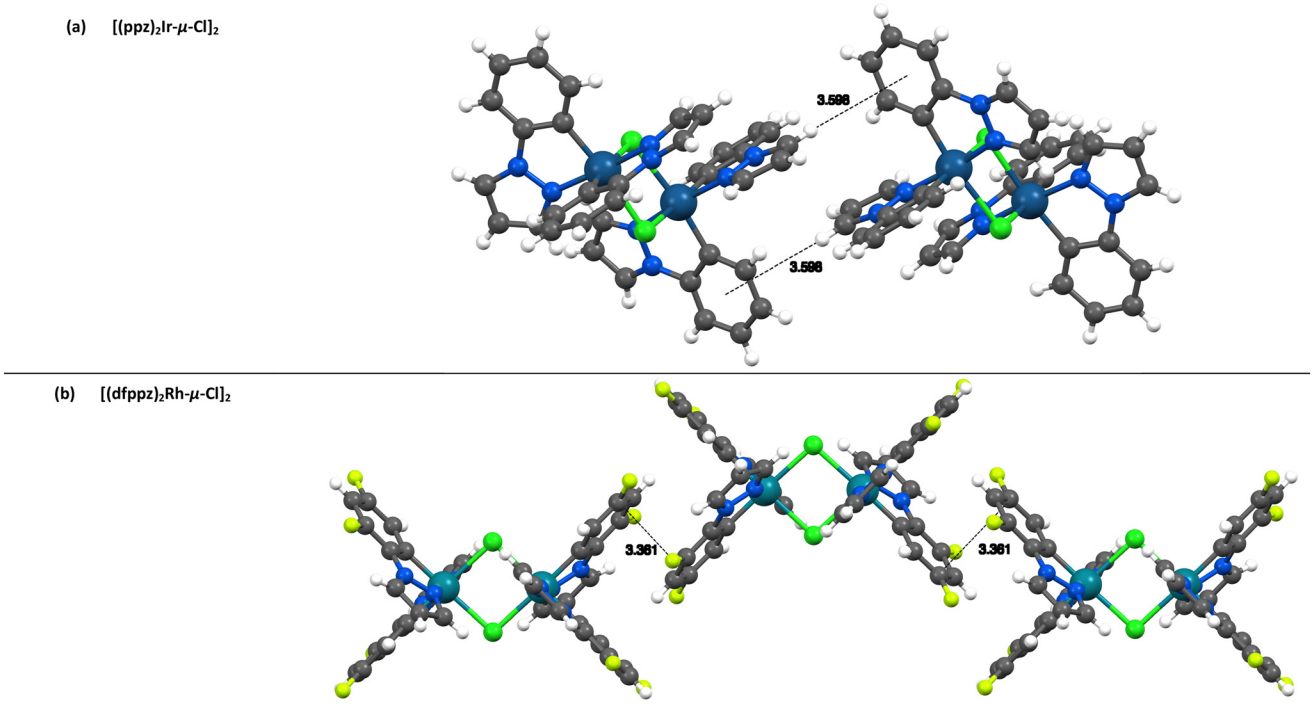

Fig. 3 C–H···π interactions in crystals of the $[(ppz)_2Ir\text{-}\mu\text{-}Cl]_2$ dinuclear complex (a) and π···π stacking interactions in crystals of the $[(dfppz)_2Rh\text{-}\mu\text{-}Cl]_2$ dinuclear complex (b). Interplanar distances between the stacking rings are presented.

Table 2 Absorption maxima and molar extinction coefficients in dichloromethane solutions, and emission properties (position of emission maxima (λ_{em}) and emission lifetimes (τ_{em})) of the investigated $[(ppz)_2M\text{-}\mu\text{-}Cl]_2$ and $[(dfppz)_2M\text{-}\mu\text{-}Cl]_2$ complexes; data obtained at 77 K in 1 : 1 MeOH/EtOH glasses

	298 K	77 K	
Complex	λ_{abs}/nm ($\varepsilon_{max}/10^4$ M^{-1} cm^{-1})	λ_{em}/nm	$^a\tau_{em}$/μs
$[(ppz)_2Ir(\mu\text{–}Cl)]_2$	241 (5.85), 313 (1.33), 365 (0.30)	633	1.93
$[(dfppz)_2Ir(\mu\text{–}Cl)]_2$	234 (6.65), 298sh (1.46), 352 (0.22)	588	4.31
$[(ppz)_2Rh(\mu\text{–}Cl)]_2$	242 (7.37), 263sh (3.83), 304 (1.68), 331 (0.58)	705	0.68
$[(dfppz)_2Rh(\mu\text{–}Cl)]_2$	238 (7.56), 268sh (2.74), 290sh (1.40), 313 (0.52)	670	0.84

[a] Marginal contribution (≈1–5%) from other components is visible.

shifted with respect to their iridium(III) counterparts (λ_{abs} = 352–365 nm). This trend is fully reproduced in the simulations. This hypsochromic shift in absorption bands from iridium(III) to rhodium(III) is consistent with the assignment of ^{1}MLCT transitions in view of the lower d_π orbital energy of the rhodium(III) center. Both the band energies of Rh(III) and Ir(III) dinuclear complexes are very close to the band energies of other complexes of these metal ions with ppz^- and $dfppz^-$ cyclometallating ligands.[26,58] The second effect observed was a hypsochromic shift of several nanometers in the MLCT bands of dinuclear complexes containing cyclometallating ligands with fluorine substituents ($dfppz^-$) relative to the bands of those with non-fluorinated ppz^- ligands (Table 2).

For more detailed information, DFT and TDDFT calculations were carried out on the optimized ground state geometries of the investigated $[(ppz)_2M\text{-}\mu\text{-}Cl]_2$ and $[(dfppz)_2M\text{-}\mu\text{-}Cl]_2$ dinuclear complexes in the presence of CH_2Cl_2 solvent. The HOMOs and LUMOs for the dichloro-bridged dinuclear complexes are shown in Fig. 5. In all complexes, the HOMOs are distributed across the metal centers, the phenyl rings of the cyclometallating ppz^- or $dfppz^-$ ligands and the chlorine bridge. The LUMOs are mainly distributed across all of the cyclometallating ligands, despite a non-negligible contribution from the M_2Cl_2 moiety. The weak band observed near the visible region of absorption spectra is contributed by $S_0 \rightarrow S_1$ absorptions, which correspond to the HOMO–LUMO transitions (with an oscillator strength (f) around 0.15 and 0.05 for Ir(III) and Rh(III) complexes, respectively). These absorptions correspond to mixed MLCT/ILCT character with some admixture of MC. The topologies for HOMO−1 and LUMO+1 are nearly identical to those of the HOMO and LUMO, respectively.

Emission properties

All investigated Rh(III) and Ir(III) dichloro-bridged dinuclear complexes do not show any noticeable emission in CH_2Cl_2 solutions at room temperature. The suppression of light emission is most likely due to their symmetry.[59] Additionally, in the case of Rh(III) complexes, emission quenching at room temperature can also occur due to a nonradiative deactivation

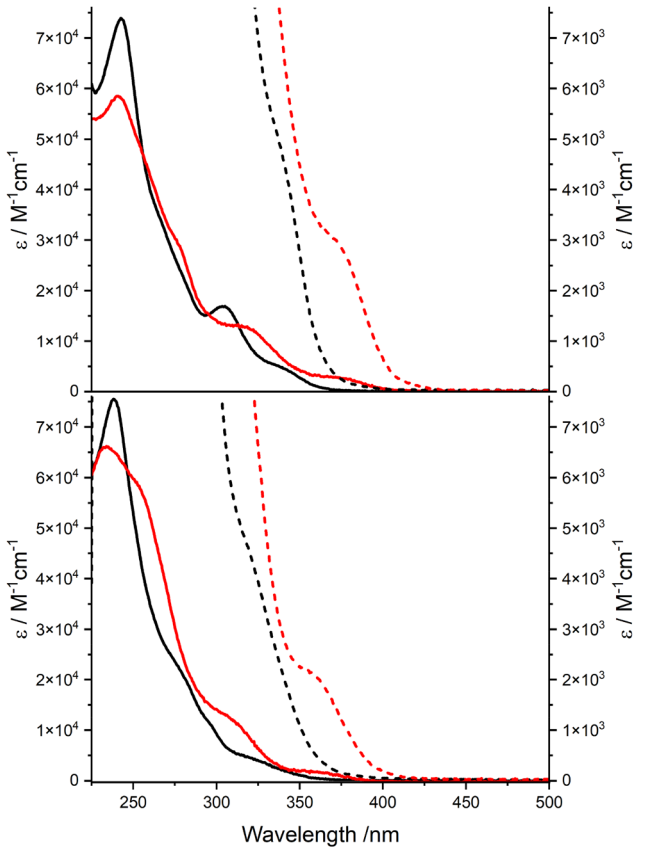

Fig. 4 Band profiles of UV-Vis absorption spectra for the $[(ppz)_2M\text{-}\mu\text{-}Cl]_2$ (top) and $[(dfppz)_2M\text{-}\mu\text{-}Cl]_2$ dinuclear complexes (bottom) in CH_2Cl_2 solutions (Rh(III) complexes – black lines, Ir(III) complexes – red lines, short dashed lines present the expanded low energy part of the spectra).

pathway by the thermal population of non-luminescent ^{3}MC (d–d) states,[54,60,61] similar to that in many cyclometallated monomeric Rh(III) complexes.[34,37,62]

At 77 K, these complexes are all emissive in 1 : 1 MeOH/EtOH matrices (Table 2, Fig. 6 and Fig. S8†). In their spectra, broad and structureless emission bands are observed. The emission spectra of $[(C\hat{}N)_2Rh\text{-}\mu\text{-}Cl]_2$ complexes are clearly shifted towards lower energies compared to the spectra of their $[(C\hat{}N)_2Ir\text{-}\mu\text{-}Cl]_2$ analogues (Table 2 and Fig. 6). The excitation spectra of the studied complexes reproduce the global shape of their absorption spectra recorded at the same concentration and in the same solvent medium (*cf.* ESI, Fig. S7†).

In the case of the Ir(III) dichloro-bridged dinuclear complexes, it is reasonable to begin a discussion of the observed luminescence properties with a comparison to the emission properties of the *fac*/*mer*-Ir(ppz)$_3$ and *fac*/*mer*-Ir(dfppz)$_3$ complexes, possessing only cyclometallating ligands ppz$^-$ or dfppz$^-$ in the coordination sphere of the central metal ion. At 77 K, these monomeric complexes are characterized by the presence of structured emission bands with rich vibrational progression ($\lambda_{em} \cong 414$–430, corresponding to the highest energy peak in the spectrum), which have been attributed to the phosphorescence from a mixed ligand-centered-MLCT (LC-MLCT) triplet state.[58,63] Under these experimental conditions, the broad and structureless emission bands of the studied Ir(III) dinuclear complexes are clearly bathochromically shifted (Fig. 6 and Table 2).

The situation is similar to the emission properties of the Rh(III) dichloro-bridged dinuclear complexes. At 77 K, the shape and position of emission bands in the Rh(III) complexes and the emission lifetimes (Fig. 6 and Table 2) are completely different from those observed in the spectra of other dichloro-bridged dinuclear complexes (*e.g.* $[(ppy)_2Rh\text{-}\mu\text{-}Cl]_2$),[47] in which highly structured bands with multiple emission maxima with very long emission lifetimes (several dozen microseconds or even several milliseconds) are observed.[25,47,52] For these dinuclear complexes, the ^{3}*IL ($\pi \rightarrow \pi^*$)(C^N$^-$) character of the emission was mainly postulated with only some admixture of ^{3}*MLCT (d_π(Rh) $\rightarrow \pi^*$(C^N$^-$)) character in some cases.[25]

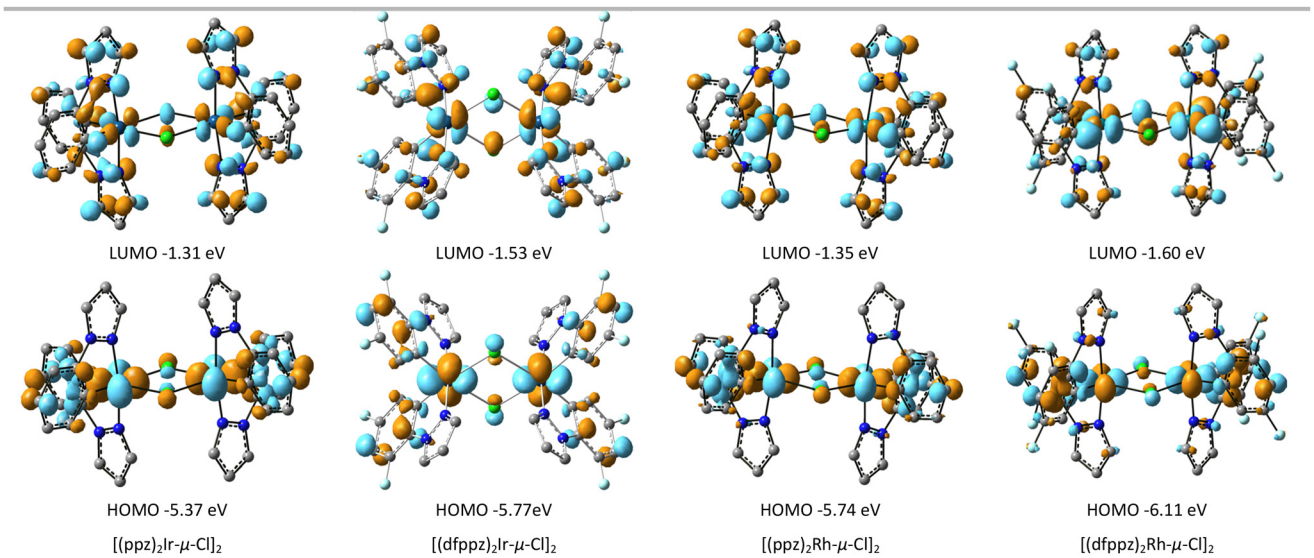

Fig. 5 Kohn–Sham HOMOs and LUMOs of all compounds with their energies in eV.

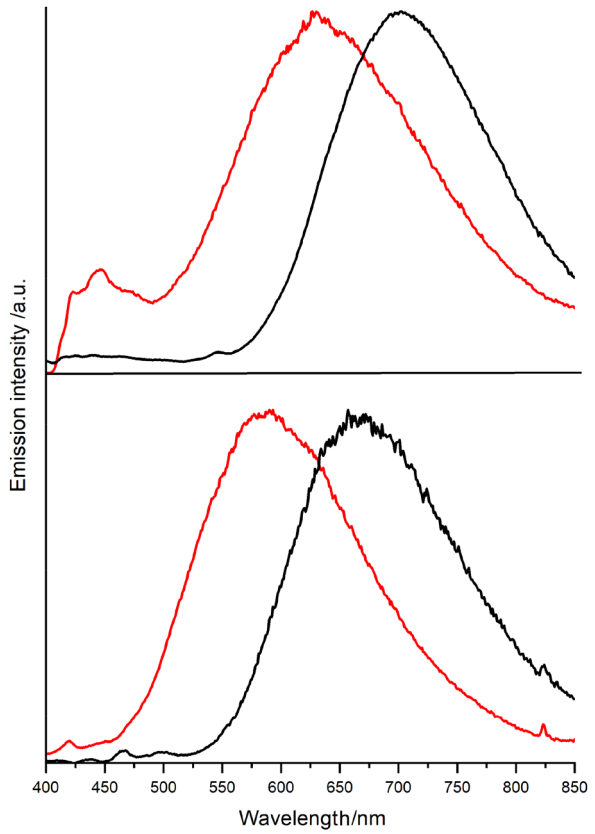

Fig. 6 Emission spectra for the $[(ppz)_2M\text{-}\mu\text{-}Cl]_2$ (top) and $[(dfppz)_2M\text{-}\mu\text{-}Cl]_2$ dinuclear complexes (bottom) in 1 : 1 MeOH/EtOH matrices at 77 K (Rh(III) complexes – black lines, Ir(III) complexes – red lines), $c \approx 3\text{–}5 \times 10^{-4}$ mol dm^{-3} (λ_{ex} = 350 nm for $[(ppz)_2Ir\text{-}\mu\text{-}Cl]_2$), λ_{ex} = 325 nm for $[(ppz)_2Rh\text{-}\mu\text{-}Cl]_2$, λ_{ex} = 340 nm for $[(dfppz)_2Ir\text{-}\mu\text{-}Cl]_2$ and λ_{ex} = 315 nm for $[(dfppz)_2Rh\text{-}\mu\text{-}Cl]_2$.

The emission spectra of the Rh(III) dinuclear complexes studied here are also different from the emission spectrum of the free ppz ligand (λ_{em} = 378 nm, $\tau_{em} > 10^5$ μs).[34,64] In accordance with the observed differences, it is possible to exclude the pure ^{3}*IL ($\pi \rightarrow \pi^*$)(ppz$^-$) nature of the emission in the case of the studied $[(ppz)_2Rh\text{-}\mu\text{-}Cl]_2$ and $[(dfppz)_2Rh\text{-}\mu\text{-}Cl]_2$ dinuclear complexes. Therefore, the nature of the excited state from which the emission occurs at 77 K in 1 : 1 MeOH/EtOH glasses must be different, especially since the energy of the phenylpyrazole triplet is higher than that of phenylpyridine (430 nm, $\tau_{em} > 10^5$ μs).[62]

To further understand the emission properties of the studied dichloro-bridged dinuclear complexes, DFT computations were performed to study the triplet states (T_0) to estimate the electronic luminescence energy together with the spin densities (Fig. S10†). It should be mentioned that the trend, a higher luminescence wavelength, going from "dfppz" to "ppz" is well reproduced in the simulations. Unfortunately, since the ground and excited states strongly differ, it is not possible to simulate the vibronic fine spectrum. However, the relaxed triplet excited state structures exhibit one broken M–Cl bond (Table 1 and Fig. S10†), indicating that the excited-state geometries strongly distort with respect to the ground state ones. The cleavage of either an Ir–Cl or Rh–Cl bond can then lead to subsequent rearrangement of the complex and explains the lack of the emission properties.[58,65]

The computed electronic vertical emission *via* DFT are, as expected, in very good agreement with respect to the experiment in the case of Ir(III) complexes and calculated to be 659 and 591 nm for the $[(ppz)_2Ir\text{-}\mu\text{-}Cl]_2$ and $[(dfppz)_2Ir\text{-}\mu\text{-}Cl]_2$ complexes, respectively (deviation < 0.10 eV).[66–68] The shape of the emission bands and their location in the wavelength range (633 and 588 nm, respectively) observed at 77 K in 1 : 1 MeOH/EtOH matrices as well as emission lifetimes (Table 2) allow us to conclude that the emission character is the same upon lowering the temperature and strongly suggest that the observed emission arises from the excited state possessing ^{3}*MLCT character.

However, for the Rh(III) complexes, the computed emission wavelengths are 615 and 605 nm and fall around 0.2 eV from experiment but remains in the accepted deviation in DFT. The emission bands of $[(ppz)_2Rh\text{-}\mu\text{-}Cl]_2$ and $[(dfppz)_2Rh\text{-}\mu\text{-}Cl]_2$ recorded at 77 K are red-shifted relative to the spectra simulated at room temperature by about 90 and 65 nm, respectively. Furthermore, these bands are also shifted towards longer wavelengths in comparison with those of Ir(III) analogues by about 70–80 nm, which is unreasonable if the typical MLCT nature of emission was assumed for Rh(III) dinuclear complexes at this temperature regime.

Thorough X-ray structural analysis (see above) may be useful in explaining the obtained results. In the crystal structure of the $[(ppz)_2Ir\text{-}\mu\text{-}Cl]$ dinuclear complex, short contacts of C–H···π (point-to-face, edge-on, T-shaped)[69] are observed at a distance of 3.598 Å (Fig. 3(a)). Similarly, the crystal structure of $[(dfppz)_2Rh\text{-}\mu\text{-}Cl]_2$ revealed π–π stacking (offset π-stacked)[69] interactions at a distance of 3.360 Å between pyridyl rings of the adjacent ppz$^-$ ligands of neighbouring molecules (Fig. 3(b)). So, it can be suggested that these interactions are also present to some extent in frozen solutions, which in turn can give the origin of the aggregation-induced emission (AIE), in particular, the latter one in the case of Rh(III) dinuclear complexes.[54,57,70] There are many reports in the literature on cyclometallated iridium(III) complexes that have been shown to be AIE-active.[70–75] This phenomenon has also recently been documented for Rh(III) complexes.[54] It has been shown that the establishment of intermolecular interactions enforces molecular rigidity in the solid state, enhancing the efficiency of the restriction of internal motion (RIM) processes blocking the non-radiative deactivation of the emitting state with the overall result of a strong emission in solid and aggregated states.[76] These interactions in the frozen solutions presumably reduce the energy of the π*ppz orbital, lowering the metal-to-ligand charge-transfer (^{3}MLCT) state from which the emission occurs, resulting in a red shift of the emission band (Fig. 6).[70] This effect is particularly pronounced in the case of Rh(III) complexes, where the offset π-stacking interactions have been detected and, consequently, the energy decrease of the emitting state and the bathochromic shift of the emission band are more significant.

On the other hand, it should be taken into account that for Rh(III) dinuclear complexes ($4d^6$), the ^{3}MLCT and ^{3}MC states have similar energies, and at 77 K, the energy order of the ^{3}MLCT and ^{3}MC states may be reversed. Consequently, the ^{3}MC state may lie below the ^{3}MLCT state. MC states have been shown to be non-emissive at room temperature. However, lowering the temperature of the solutions to 77 K before excitation of the complex sample may prevent the strong distortion in the excited state and it cannot be excluded that the observed emission in this temperature regime for Rh(III) dinuclear complexes is MC in nature.

Conclusions

In conclusion, four dichloro-bridged dinuclear iridium(III) complexes and two of their Rh(III) analogues were synthesized and characterized experimentally and theoretically. The molecular structures of the studied Rh(III) and Ir(III) analogues are very similar and the complexes adopt a slightly distorted octahedral coordination environment around the metal(III) centres, with M–N being *trans* to each other and M–C being *cis*. In the crystal structures of the studied $[(ppz)_2Ir\text{-}\mu\text{-}Cl]_2$ and $[(dfppz)_2Rh\text{-}\mu\text{-}Cl]_2$ dinuclear complexes, intermolecular interactions were identified: π···π stacking in the structure of the former and C–H···π interactions in the structure of the latter. Although the absorption spectral profiles of the iridium(III) and rhodium(III) dinuclear complexes are quite similar, due to the lower energy of the d_π orbitals, a hypsochromic shift of the lowest energy band (^{1}MLCT) of the $[(C\hat{}N)_2Rh\text{-}\mu\text{-}Cl]_2$ dinuclear complexes is observed with respect to their $[(C\hat{}N)_2Ir\text{-}\mu\text{-}Cl]_2$ analogues. The luminescence properties of both types of dinuclear complexes, Ir(III) and Rh(III), containing the same cyclometallating ligands were compared. At room temperature, these dinuclear complexes are non-emissive complexes, while at 77 K, emission of these complexes is observed, and the emission bands are broad and structureless. Based on theoretical calculations, an analysis of the observed emission properties was carried out, and the nature of the emitting state was proposed.

Experimental

Materials

Unless otherwise stated, all chemicals and reagents were obtained from TCI, Sigma–Aldrich, Alfa Aesar, Fluorochem and Merck, and used without further purification in the syntheses and purification of the investigated complexes. 1-Phenyl-1*H*-pyrazole was purchased from TCI, >97%, rhodium(III) chloride from Sigma–Aldrich, iridium(III) chloride from Alfa Aesar, and 1,1,3,3-tetraethoxypropan and 2,4-(difluorophenyl)hydrazine hydrochloride from Fluorochem, respectively. Solvents used in UV-VIS absorption and emission studies, such as dichloromethane, methanol, and ethanol, specially designed for spectroscopic studies of the highest spectral purity Uvasol®, were purchased from Merck. The Hdfppz cyclometallating ligand was synthesized according to a reported procedure.[89]

Instrumentation

^{1}H and ^{13}C NMR spectra were recorded using a VARIAN 400-MR NMR spectrometer. The chemical shifts (δ) of ^{1}H-NMR were referenced to the residual solvent shift in the deuterated solvent. Elemental analysis (CHN) for carbon, hydrogen and nitrogen was performed on an Elementar Vario Micro Cube analyzer. UV-Vis absorption spectra were measured with a Shimadzu UV 3100 spectrometer in the range of 200–600 nm in spectroscopically pure-grade organic solvent (DCM and 1 : 1 MeOH/EtOH). Corrected steady-state luminescence spectra were recorded with a Gilden Photonics FluoroSense fluorimeter. In the case of emission studies at 298 K, the investigated CH_2Cl_2 solutions of the complexes, placed in fluorimeter quartz cuvettes (1 × 1 cm), were carefully deaerated before measurement by prolonged saturation with preliminarily purified and dried argon. In turn, 77 K measurements were performed in NMR-like fused silica tubes with a 3 mm inner diameter by placing them in a liquid nitrogen-filled Dewar flask with a bottom transparent finger. Emission decays were recorded with a FluoroSense-P fluorimeter especially designed for time-resolved measurements in the microsecond range with the temporal resolution of 0.01 μs. In the performed lifetime measurements, the investigated samples were excited at 350 nm, whereas emission signals were recorded at the wavelengths corresponding to the maxima of steady-state emissions. The experimental decay curves were analyzed by the single-curve method using the reference convolution based on the Marquardt algorithm[77] with χ^2 values. The distributions of residuals and the adjusted coefficients of determination R^2 values served as the criteria in the evaluation of the fit quality. Lifetime τ_{em} values were determined with an estimated error of *ca.* ±10%.

Computational details

All the computations have been performed using the Gaussian 16 package[78] using the B3PW91[79–81] together with the LANL2DZ basis set, which includes a pseudopotential to describe core electrons for large atoms, augmented by polarization functions on all atoms except hydrogens.[66,82–84] Relativistic effects have not been explicitly taken into account. The solvent effects (CH_2Cl_2) have been modelled using the PCM[85] solvation regime within the UAKS topological model. All the ground and excited state structures have been optimized and checked to be at a true minimum on the potential energy surface by diagonalizing the Hessian (no imaginary frequency), except for $[(ppz)_2Rh\text{-}\mu\text{-}Cl]_2$, where a very small ($4i$) imaginary frequency at the triplet excited state has been ignored. The absorption spectra have been simulated with the Time-Dependent DFT (TDDFT) methodology. Triplet excited state structures have been relaxed using either the TDDFT or the unrestricted method.

X-ray structure determination

The X-ray data were collected on a Bruker D8 FIXEDCHI diffractometer with a microfocus sealed tube using a multilayer mirror as a monochromator and a PhotonII_7 CPAD detector. The diffractometer was equipped with a Cryostream low temperature device and used Mo Kα radiation (λ = 0.71073 Å). A multi-scan absorption correction using SADABS 2016/2 was applied.[86] The structures were solved by intrinsic phasing methods with SHELXT 2018/2 and refined by full-matrix least-squares methods against F^2 using SHELXL-2019/2.[87,88] All non-hydrogen atoms were refined with anisotropic displacement parameters. All hydrogen atoms were refined isotropically on calculated positions using a riding model with their U_{iso} values constrained to 1.5 times the U_{eq} of their pivot atoms for terminal sp^3 carbon atoms and 1.2 times for all other carbon atoms. CCDC 2431406 and 2431407† contain the supplementary crystallographic data for this paper.

Synthesis of the compounds

Synthesis of $[(C^N)_2Ir\text{-}\mu\text{-}Cl]_2$ complexes. Both the dichloro-bridged Ir(III) dinuclear complexes ($[(ppz)_2Ir\text{-}\mu\text{-}Cl]_2$ and $[(dfppz)_2Ir\text{-}\mu\text{-}Cl]_2$) were obtained using similar synthesis conditions and substrate amounts to those described earlier.[35] $IrCl_3{\cdot}3H_2O$ (600 mg, 1.72 mmol) and the appropriate cyclometallating ligand, Hppz or Hdfppz, (~3 equiv.) were heated in a mixture of 2-ethoxyethanol : water (v/v = 3 : 1, 36 mL) under an argon atmosphere at 110 °C for 24 h to form a yellow solution. After cooling to room temperature, deionized water was added to the reaction mixture under stirring. The suspension was then filtered followed by washing with deionized water and ethanol to afford the corresponding dinuclear dichloro-bridged complex. The filter residue was dried, giving a light-yellow powder. In order to obtain spectroscopically pure complexes suitable for photophysical studies, the resulting crude products were purified by column chromatography using silica gel 60 (63–200 μm mesh) with CH_2Cl_2 followed by a CH_2Cl_2/MeOH (100 : 1) mixture as the eluent. The isolated complexes were then recrystallized from dichloromethane/methanol giving pale yellow, block-shaped crystals. The NMR spectra are consistent with the literature data.[43,58,90]

$[(ppz)_2Ir\text{-}\mu\text{-}Cl]_2$. Yield: 86%. ^{1}H NMR (400 MHz, CD_2Cl_2, ppm): δ 8.20 (4H, dd, J = 2.9, 0.7 Hz, H_e of the pyrazole ring), 7.84 (4H, dd, J = 2.3, 0.7 Hz, H_g of the pyrazole ring), 7.20 (4H, dd, J = 7.9, 1.2 Hz, H_d of the phenyl ring), 6.85 (4H, td, J = 7.6, 1.3 Hz, H_c of the phenyl ring), 6.70 (4H, dd, J = 2.9, 2.2 Hz, H_f of the pyrazole ring), 6.58 (4H, td, J = 7.5, 1.3 Hz, H_b of the phenyl ring), 5.96 (4H, dd, J = 7.7, 1.2 Hz, H_a of the phenyl ring) (28 protons). $^{13}C\{^1H\}$ NMR (400 MHz, CD_2Cl_2, ppm): δ 143.50 (C_i), 140.85 (C_g), 132.83 (C_a), 127.73 (C_h), 126.81 (C_e), 125.57 (C_b), 122.31 (C_c), 110.98 (C_d), 107.08 (C_f) (9 signals). Anal. calc. (%) for $C_{36}H_{28}N_8Cl_2Ir_2$: C, 42.06; H, 2.74; N, 10.90. Found: C, 42.10; H, 2.41; N, 10.87.

$[(dfppz)_2Ir\text{-}\mu\text{-}Cl]_2$. Yield: 83%. ^{1}H NMR (400 MHz, CD_2Cl_2, ppm): δ 8.47 (4H, d, J = 2.9 Hz, H_e of the pyrazole ring), 7.77 (4H, d, J = 2.3 Hz, H_g of the pyrazole ring), 6.75 (4H, dd, J = 2.9, 2.3 Hz, H_f of the pyrazole ring), 6.50 (4H, ddd, J = 12.0, 8.9, 2.5 Hz, H_c of the phenyl ring), 5.39 (4H, ddd, J = 8.6, 2.5, 0.9 Hz, H_a of the phenyl ring) (20 protons). $^{13}C\{^1H\}$ NMR (400 MHz, CD_2Cl_2, ppm): δ 159.31 (dd, J_{C-F} = 250.0, 10.9 Hz, C_b), 148.62 (dd, J_{C-F} = 252.2, 13.2 Hz, C_d), 140.53 (C_g), 131.72 (d, J_{C-F} = 14.8 Hz, C_i), 131.41 (d, J_{C-F} = 6.6 Hz, C_e), 127.78 (dd, J_{C-F} = 5.0, 3.0 Hz, C_h), 114.66 (dd, J_{C-F} = 19.7, 2.5 Hz, C_a), 107.97 (d, J_{C-F} = 2.2 Hz, C_f), 98.63 (dd, J_{C-F} = 28.1, 23.7 Hz, C_c) (9 signals). Anal. calc. (%) for $C_{36}H_{20}N_8F_8Cl_2Ir_2$: C, 36.895; H, 1.72; N, 9.56. Found: C, 37.18; H, 1.56; N, 9.74.

Synthesis of $[(C^N)_2Rh\text{-}\mu\text{-}Cl]_2$ complexes. The dichloro-bridged $[(ppz)_2Rh\text{-}\mu\text{-}Cl]_2$ and $[(dfppz)_2Rh\text{-}\mu\text{-}Cl]_2$ complexes were obtained using the synthetic route described earlier.[37] $RhCl_3{\cdot}H_2O$ (409 mg, 1.80 mmol) and Hppz or Hdfppz (~4 equiv.) were heated in a mixture of ethanol–water (v/v = 3 : 1, 60 mL) under an argon atmosphere at 80 °C for 24 h. After cooling down the reaction mixture to room temperature, the precipitate was filtered off and washed with diethyl ether. The crude product was purified by column chromatography on silica gel 60 (63–200 μm mesh) with CH_2Cl_2 as the eluent. The elution of the complexes was controlled by analytical thin-layer-chromatography with TLC silica gel 60 on aluminium sheets (F-254 indicator). TLC visualization was accomplished using a 254/365 nm UV lamp. The eluted dichloro-bridged complexes were recrystallized from dichloromethane/ethanol giving colourless, block-shaped crystals.

$[(ppz)_2Rh\text{-}\mu\text{-}Cl]_2$. Yield: 55%. ^{1}H NMR (400 MHz, CD_2Cl_2, ppm): δ 8.24 (4H, d, J = 2.9 Hz, H_e of the pyrazole ring), 7.87 (4H, d, J 2.2 Hz, H_g of the pyrazole ring), 7.22 (4H, dd, J = 7.9, 1.3 Hz, H_d of the phenyl ring), 6.93 (4H, td, J = 7.6, 1.3 Hz, H_c of the phenyl ring), 6.67 (4H, td, J = 7.5, 1.3 Hz, H_b of the phenyl ring), 6.59 (4H, dd, J = 2.8, 2.2 Hz, H_f of the pyrazole ring), 5.98 (4H, dt, J = 7.7, 1.3 Hz, H_a of the phenyl ring) (28 protons). $^{13}C\{^1H\}$ NMR (400 MHz, CD_2Cl_2, ppm): δ 147.70 (d, J_{C-Rh} = 35.7 Hz, C_i), 142.53 (C_h), 141.60 (C_g), 133.97 (C_a), 126.27 (C_e), 125.75 (C_b), 123.19 (C_c), 111.62 (C_d), 107.58 (C_f) (9 signals). Anal. calc. (%) for $C_{36}H_{28}N_8Cl_2Rh_2$: C, 50.91; H, 3.32; N, 13.19. Found: C, 50.80; H, 3.03; N, 13.34.

$[(dfppz)_2Rh\text{-}\mu\text{-}Cl]_2$. Yield: 48%. ^{1}H NMR (400 MHz, CD_2Cl_2, ppm): δ 8.49 (4H, d, J = 2.9 Hz, H_e of the pyrazole ring), 7.80 (4H, d, J = 2.3 Hz, H_g of the pyrazole ring), 6.65 (4H, dd, J = 2.9, 2.3 Hz, H_f of the pyrazole ring), 6.54 (4H, ddd, J = 11.9, 8.7, 2.5 Hz, H_c of the phenyl ring), 5.44 (4H, ddt, J = 8.3, 2.7, 1.3 Hz, Ha of the phenyl ring) (20 protons). $^{13}C\{^1H\}$ NMR (400 MHz, CD_2Cl_2, ppm): δ 158.82 (ddd, J_{C-F} = 251.1, 10.3, 3.1 Hz, C_b), 151.32 (ddd, J_{C-Rh} = 35.7 Hz, J_{C-F} = 6.2, 2.2 Hz, C_i), 148.92 (dd, J_{C-F} = 253.3, 12.5 Hz, C_d), 141.25 (C_g), 131.32 (d, J_{C-F} = 14.9 Hz, C_e), 126.78 (C_h), 115.61 (dd, J_{C-F} = 20.3, 2.9 Hz, C_a), 108.46 (d, J_{C-F} = 1.8 Hz, C_f), 99.69 (dd, J_{C-F} = 28.2, 23.6 Hz, C_c) (9 signals). Anal. calc. (%) for $C_{36}H_{20}N_8F_8Cl_2Rh_2$: C, 43.53; H, 2.03; N, 11.28. Found: C, 43.77; H, 1.81; N, 11.37.

Author contributions

P. W.: methodology, investigation, data curation, and visualization. C. L.: methodology, formal analysis, investi-

gation, data curation, visualization, and writing – review & editing. K. S.: methodology, formal analysis, investigation, data curation, validation, and writing – review & editing. A. K.: conceptualization, methodology, validation, formal analysis, investigation, resources, data curation, writing – original draft, writing – review & editing, and visualization.

Conflicts of interest

There are no conflicts to declare.

Data availability

All experimental and computational data supporting the findings of this study are included in the article and the ESI.† Additional raw data or input/output files from quantum chemical calculations are available from the corresponding author upon reasonable request.

Acknowledgements

CL thanks the IUF for support and CCIPL for computational facilities.

References

1 *Iridium(III) in Optoelectronic and Photonics Applications*, ed. E. Zysman-Colman, Wiley, 2017.
2 E. Longhi and L. De Cola, in *Iridium(III) in Optoelectronic and Photonics Applications*, Wiley, 2017, pp. 205–274.
3 X. Yang, S. Xu, Y. Zhang, C. Zhu, L. Cui, G. Zhou, Z. Chen and Y. Sun, *Angew. Chem., Int. Ed.*, 2023, **62**, e202309739.
4 M. Wu, N. Li, C. Shi, J. Song, R. Zeng, F. Li, Q. Li, A. Yuan and C. Yang, *Inorg. Chem. Front.*, 2023, **10**, 1262–1269.
5 A. F. Henwood and E. Zysman-Colman, in *Iridium(III) in Optoelectronic and Photonics Applications*, Wiley, 2017, pp. 275–357.
6 C. E. Housecroft and E. C. Constable, *Coord. Chem. Rev.*, 2017, **350**, 155–177.
7 R. Bai, X. Meng, X. Wang and L. He, *Adv. Funct. Mater.*, 2021, **31**, 1–12.
8 H. L. Benford, J. C. Frith, S. Auriola, J. Mönkkönen and M. J. Rogers, *Mol. Pharmacol.*, 1999, **56**, 131–140.
9 K. K. Tso and K. K. Lo, in *Iridium(III) in Optoelectronic and Photonics Applications*, Wiley, 2017, pp. 415–477.
10 L. C. C. Lee and K. K. W. Lo, *Chem. Rev.*, 2024, **124**, 8825–9014.
11 J. Zhou, J. Li, K. Y. Zhang, S. Liu and Q. Zhao, *Coord. Chem. Rev.*, 2022, **453**, 214334.
12 T. M. Monos and C. R. J. Stephenson, in *Iridium(III) in Optoelectronic and Photonics Applications*, Wiley, 2017, pp. 541–581.
13 Y. Chen, C. Liang, M. Kou, X. Tang and J. Ru, *Dalton Trans.*, 2024, **53**, 11836–11849.
14 Z. Fan, J. Xie, T. Sadhukhan, C. Liang, C. Huang, W. Li, T. Li, P. Zhang, S. Banerjee, K. Raghavachari and H. Huang, *Chem. – Eur. J.*, 2022, **28**, e202103346.
15 J. M. Thomsen, D. L. Huang, R. H. Crabtree and G. W. Brudvig, *Dalton Trans.*, 2015, **44**, 12452–12472.
16 I. Corbucci, K. Ellingwood, L. Fagiolari, C. Zuccaccia, F. Elisei, P. L. Gentili and A. Macchioni, *Catal. Today*, 2017, **290**, 10–18.
17 J. Gao, Y. Liu, B. Liu and K.-W. Huang, *ACS Nano*, 2022, **16**, 17761–17777.
18 F. Monti, A. Baschieri, L. Sambri and N. Armaroli, *Acc. Chem. Res.*, 2021, **54**, 1492–1505.
19 S. DiLuzio, V. Mdluli, T. U. Connell, J. Lewis, V. VanBenschoten and S. Bernhard, *J. Am. Chem. Soc.*, 2021, **143**, 1179–1194.
20 D. Ma, H. He, K. Leung, D. S. Chan and C. Leung, *Angew. Chem., Int. Ed.*, 2013, **52**, 7666–7682.
21 D.-L. Ma, M. Wang, Z. Mao, C. Yang, C.-T. Ng and C.-H. Leung, *Dalton Trans.*, 2016, **45**, 2762–2771.
22 J. Ohata and Z. T. Ball, *Dalton Trans.*, 2018, **47**, 14855–14860.
23 M. Sohrabi, M. Saeedi, B. Larijani and M. Mahdavi, *Eur. J. Med. Chem.*, 2021, **216**, 113308.
24 M. Sohrabi, M. Bikhof Torbati, M. Lutz, S. Meghdadi, H. Farrokhpour, A. Amiri and M. Amirnasr, *J. Photochem. Photobiol., A*, 2022, **423**, 113573.
25 K. K.-W. Lo, C.-K. Li, K.-W. Lau and N. Zhu, *Dalton Trans.*, 2003, **3**, 4682.
26 E. V. Ivanova, M. V. Puzyk and K. P. Balashev, *Opt. Spectrosc.*, 2009, **107**, 101–105.
27 M. Graf, Y. Gothe, N. Metzler-Nolte, R. Czerwieniec and K. Sünkel, *J. Organomet. Chem.*, 2014, **765**, 46–52.
28 H. Liang, T. Hao, C. Yin, X. Yang, H. Fu, X. Zheng, R. Li, D. Xiao and H. Chen, *Eur. J. Inorg. Chem.*, 2017, **2017**, 4149–4157.
29 H. Böttcher, M. Graf and P. Mayer, *Z. Anorg. Allg. Chem.*, 2015, **641**, 1856–1858.
30 M. Graf, Y. Gothe, N. Metzler-nolte, R. Czerwieniec and K. Sünkel, *Inorg. Chim. Acta*, 2017, **463**, 36–43.
31 S. Pal, S. Joy, H. Paul, S. Banerjee, A. Maji, E. Zangrando and P. Chattopadhyay, *J. Phys. Chem. C*, 2017, **121**, 11632–11642.
32 Y. Ohsawa, S. Sprouse, K. A. King, M. K. DeArmond, K. W. Hanck and R. J. Watts, *J. Phys. Chem.*, 1987, **91**, 1047–1054.
33 D. Sandrini, M. Maestri, V. Balzani, U. Maeder and A. Von Zelewsky, *Inorg. Chem.*, 1988, **27**, 2640–2643.
34 D. Sandrini, M. Maestri, M. Ciano, U. Maeder and A. von Zelewsky, *Helv. Chim. Acta*, 1990, **73**, 1306–1313.
35 A. Kamecka, A. Kapturkiewicz and Ł. Pipczyński, *Inorg. Chem. Commun.*, 2021, **131**, 108764.
36 A. Kapturkiewicz and A. Kamecka, *RSC Adv.*, 2021, **11**, 29308–29322.
37 A. Kamecka, A. Kapturkiewicz, P. Wójcik, K. Suwińska, J. Masternak and N. Barbarczyk, *Struct. Chem.*, 2025, **36**, 709–722.

38 M. Nonoyama, *J. Organomet. Chem.*, 1975, **86**, 263–267.
39 B. Orwat, M. J. Oh, M. Zaranek, M. Kubicki, R. Januszewski and I. Kownacki, *Inorg. Chem.*, 2020, **59**, 9163–9176.
40 C. R. Groom, I. J. Bruno, M. P. Lightfoot and S. C. Ward, *Acta Crystallogr., Sect. B:Struct. Sci., Cryst. Eng. Mater.*, 2016, **72**, 171–179.
41 D. L. Davies, M. P. Lowe, K. S. Ryder, K. Singh and S. Singh, *Dalton Trans.*, 2011, **40**, 1028–1030.
42 J. Masternak, K. Okła, A. Kubas, J. Voller, K. Kozlanská, M. Zienkiewicz-Machnik, A. Gilewska, J. Sitkowski, A. Kamecka, K. Kazimierczuk and B. Barszcz, *Dalton Trans.*, 2024, **53**, 14438–14450.
43 E. Baranoff, H. J. Bolink, E. C. Constable, M. Delgado, D. Häussinger, C. E. Housecroft, M. K. Nazeeruddin, M. Neuburger, E. Ortí, G. E. Schneider, D. Tordera, R. M. Walliser and J. A. Zampese, *Dalton Trans.*, 2013, **42**, 1073–1087.
44 P. J. Steel, *J. Organomet. Chem.*, 1991, **408**, 395–402.
45 A. M'hamedi, A. S. Batsanov, M. A. Fox, M. R. Bryce, K. Abdullah, H. A. Al-Attar and A. P. Monkman, *J. Mater. Chem.*, 2012, **22**, 13529.
46 M. Y. Wong, G. Xie, C. Tourbillon, M. Sandroni, D. B. Cordes, A. M. Z. Slawin, I. D. W. Samuel and E. Zysman-Colman, *Dalton Trans.*, 2015, **44**, 8419–8432.
47 S. Sprouse, K. A. King, P. J. Spellane and R. J. Watts, *J. Am. Chem. Soc.*, 1984, **106**, 6647–6653.
48 F. O. Garces, K. A. King and R. J. Watts, *Inorg. Chem.*, 1988, **27**, 3464–3471.
49 G. A. Carlson, P. I. Djurovich and R. J. Watts, *Inorg. Chem.*, 1993, **32**, 4483–4484.
50 S. Lamansky, P. Djurovich, D. Murphy, F. Abdel-Razzaq, R. Kwong, I. Tsyba, M. Bortz, B. Mui, R. Bau and M. E. Thompson, *Inorg. Chem.*, 2001, **40**, 1704–1711.
51 S. Bettington, M. Tavasli, M. R. Bryce, A. S. Batsanov, A. L. Thompson, H. A. Al Attar, F. B. Dias and A. P. Monkman, *J. Mater. Chem.*, 2006, **16**, 1046–1052.
52 L. Ghizdavu, O. Lentzen, S. Schumm, A. Brodkorb, C. Moucheron and A. Kirsch-De Mesmaeker, *Inorg. Chem.*, 2003, **42**, 1935–1944.
53 R. D. Shannon, *Acta Crystallogr.*, 1976, **A32**, 751–767.
54 M. A. Kiseleva, A. V. Churakov, I. V. Taydakov, M. T. Metlin, S. A. Kozyukhin and S. I. Bezzubov, *Dalton Trans.*, 2023, **52**, 17861–17872.
55 E. S. Andreiadis, D. Imbert, J. Pécaut, A. Calborean, I. Ciofini, C. Adamo, R. Demadrille and M. Mazzanti, *Inorg. Chem.*, 2011, **50**, 8197–8206.
56 O. Chepelin, J. Ujma, X. Wu, A. M. Z. Slawin, M. B. Pitak, S. J. Coles, J. Michel, A. C. Jones, P. E. Barran and P. J. Lusby, *J. Am. Chem. Soc.*, 2012, **134**, 19334–19337.
57 Q. Zhao, L. Li, F. Li, M. Yu, Z. Liu, T. Yi and C. Huang, *Chem. Commun.*, 2008, **3**, 685–687.
58 A. B. Tamayo, B. D. Alleyne, P. I. Djurovich, S. Lamansky, I. Tsyba, N. N. Ho, R. Bau and M. E. Thompson, *J. Am. Chem. Soc.*, 2003, **125**, 7377–7387.
59 M.-X. Song, Y. Li, D. Xu, R.-P. Deng, F.-Q. Bai and Z.-K. Qin, *RSC Adv.*, 2016, **6**, 68960–68963.
60 F. Barigelletti, D. Sandrini, M. Maestri, V. Balzani, A. Von Zelewsky, L. Chassot, P. Jolliet and U. Maeder, *Inorg. Chem.*, 1988, **27**, 3644–3647.
61 I. B. Losada and P. Persson, *Chem. Sci.*, 2023, **14**, 13713–13721.
62 M. Maestri, D. Sandrini, V. Balzani, U. Maeder and A. Von Zelewsky, *Inorg. Chem.*, 1987, **26**, 1323–1327.
63 T. Sajoto, P. I. Djurovich, A. Tamayo, M. Yousufuddin, R. Bau, M. E. Thompson, R. J. Holmes and S. R. Forrest, *Inorg. Chem.*, 2005, **44**, 7992–8003.
64 J. W. Pavlik, R. E. Connors, D. S. Burns and E. M. Kurzweil, *J. Am. Chem. Soc.*, 1993, **115**, 7645–7652.
65 S. Pal, S. Joy, H. Paul, S. Banerjee, A. Maji, E. Zangrando and P. Chattopadhyay, *J. Phys. Chem. C*, 2017, **121**, 11632–11642.
66 R. Schira and C. Latouche, *Dalton Trans.*, 2021, **50**, 746–753.
67 E. Martínez-Vollbert, C. Philouze, T. Cavignac, C. Latouche, F. Loiseau and P.-H. Lanoë, *Dalton Trans.*, 2024, **53**, 4705–4718.
68 F. Vazart and C. Latouche, *Theor. Chem. Acc.*, 2015, **134**, 144.
69 C. Janiak, *J. Chem. Soc., Dalton Trans.*, 2000, 3885–3896.
70 P. Alam, C. Climent, P. Alemany and I. R. Laskar, *J. Photochem. Photobiol., C*, 2019, **41**, 100317.
71 A. Fermi, P. Ceroni and I. R. Laskar, *Dalton Trans.*, 2023, **52**, 10637–10638.
72 A. Agarwal, R. P. Bhatta, V. Kachwal and I. R. Laskar, *Dalton Trans.*, 2023, **52**, 14182–14193.
73 Y.-M. Chen, A.-G. Zhang, Y.-J. Liu and K.-Z. Wang, *J. Organomet. Chem.*, 2011, **696**, 1716–1722.
74 S. Liu, J. Han, W. Wang, Y. Chang, R. Wang, Z. Wang, G. Li, D. Zhu and M. R. Bryce, *Dalton Trans.*, 2022, **51**, 16119–16125.
75 J. Tong, X. Yang, X. Song, J. Liang, S. Huang, H. Mao, M. Akhtar, A. Liu, G.-G. Shan and G. Li, *Dalton Trans.*, 2023, **52**, 1105–1112.
76 P. Alam, S. Dash, C. Climent, G. Kaur, A. R. Choudhury, D. Casanova, P. Alemany, R. Chowdhury and I. R. Laskar, *RSC Adv.*, 2017, **7**, 5642–5648.
77 D. W. Marquardt, *J. Soc. Ind. Appl. Math.*, 1963, **11**, 431–441.
78 M. J. Frisch, G. W. Trucks, H. B. Schlegel, G. E. Scuseria, M. A. Robb, J. R. Cheeseman, G. Scalmani, V. Barone, G. A. Petersson, H. Nakatsuji, X. Li, M. Caricato, A. V. Marenich, J. Bloino, B. G. Janesko, R. Gomperts, B. Mennucci, H. P. Hratchian, J. V. Ortiz, A. F. Izmaylov, J. L. Sonnenberg, D. Williams-Young, F. Ding, F. Lipparini, F. Egidi, J. Goings, B. Peng, A. Petrone, T. Henderson, D. Ranasinghe, V. G. Zakrzewski, J. Gao, N. Rega, G. Zheng, W. Liang, M. Hada, M. Ehara, K. Toyota, R. Fukuda, J. Hasegawa, M. Ishida, T. Nakajima, Y. Honda, O. Kitao, H. Nakai, T. Vreven, K. Throssell, J. A. Montgomery Jr., J. E. Peralta, F. Ogliaro, M. J. Bearpark, J. J. Heyd, E. N. Brothers, K. N. Kudin, V. N. Staroverov, T. A. Keith, R. Kobayashi, J. Normand, K. Raghavachari, A. P. Rendell,

J. C. Burant, S. S. Iyengar, J. Tomasi, M. Cossi, J. M. Millam, M. Klene, C. Adamo, R. Cammi, J. W. Ochterski, R. L. Martin, K. Morokuma, O. Farkas, J. B. Foresman and D. J. Fox, *Gaussian 16, Revision C.01*, Gaussian, Inc., Wallingford CT, 2016.
79 J. P. Perdew, K. Burke and Y. Wang, *Phys. Rev. B:Condens. Matter Mater. Phys.*, 1996, **54**, 16533–16539.
80 J. P. Perdew, *Phys. Rev. B:Condens. Matter Mater. Phys.*, 1986, **33**, 8822–8824.
81 A. D. Becke, *J. Chem. Phys.*, 1993, **98**, 5648–5652.
82 P. J. Hay and W. R. Wadt, *J. Chem. Phys.*, 1985, **82**, 270–283.
83 P. J. Hay and W. R. Wadt, *J. Chem. Phys.*, 1985, **82**, 299–310.
84 W. R. Wadt and P. J. Hay, *J. Chem. Phys.*, 1985, **82**, 284–298.
85 B. Mennucci, J. Tomasi, R. Cammi, J. R. Cheeseman, M. J. Frisch, F. J. Devlin, S. Gabriel and P. J. Stephens, *J. Phys. Chem. A*, 2002, **106**, 6102–6113.
86 L. Krause, R. Herbst-Irmer, G. M. Sheldrick and D. Stalke, *J. Appl. Crystallogr.*, 2015, **48**, 3–10.
87 G. M. Sheldrick, *Acta Crystallogr., Sect. A:Found. Adv.*, 2015, **71**, 3–8.
88 G. M. Sheldrick, *Acta Crystallogr., Sect. C:Struct. Chem.*, 2015, **71**, 3–8.
89 L. He, L. Duan, J. Qiao, G. Dong, L. Wang and Y. Qiu, *Chem. Mater.*, 2010, **22**, 3535–3542.
90 D. L. Davies, M. P. Lowe, K. S. Ryder, K. Singh and S. Singh, *Dalton Trans.*, 2011, **40**, 1028–1030.